Exotic quantum phase transitions of strongly interacting topological insulators

Kevin Slagle, Yi-Zhuang You, and Cenke Xu
Department of Physics, University of California, Santa Barbara, California 93106, USA
(Received 22 December 2014; published 11 March 2015)

Using determinant quantum Monte Carlo simulations, we demonstrate that an extended Hubbard model on a bilayer honeycomb lattice has two novel quantum phase transitions. The first is a quantum phase transition between the weakly interacting gapless Dirac fermion phase and a strongly interacting fully gapped and symmetric trivial phase, which cannot be described by the standard Gross-Neveu model. The second is a quantum critical point between a quantum spin Hall insulator with spin S^z conservation and the previously mentioned strongly interacting fully gapped phase. At the latter quantum critical point the single-particle excitations remain gapped, while spin and charge gaps both close. We argue that the first quantum phase transition is related to the $\mathbb{Z}_{16}$ classification of the topological superconductor ^{3}He-B phase with interactions, while the second quantum phase transition is a topological phase transition described by a bosonic $O(4)$ nonlinear sigma model field theory with a Θ term.

DOI: 10.1103/PhysRevB.91.115121 PACS number(s): 64.70.Tg, 73.43.Cd, 02.70.Ss

I. INTRODUCTION

The interplay between topology and interactions can lead to very rich new physics. For bosonic systems, it is understood that strong interactions can lead to many symmetry-protected topological (SPT) phases [1,2] that are fundamentally different from the standard Mott insulator and superfluid phases. In addition to producing various topological orders, for fermionic systems strong interactions can also reduce the classification of free fermion topological insulators and superconductors [3–11]. That is, interactions can drive free fermion topological superconductors to a trivial phase; namely the edge states of the free fermion topological superconductor can be gapped out without degeneracy by symmetry-preserving short-range interactions without going through a bulk quantum phase transition. The most famous example is the ^{3}He-B topological superconductor protected by time-reversal symmetry, whose boundary is described by a $(2+1)d$ Majorana fermion χ with the Hamiltonian $H = \int d^2x\ \chi^\intercal(i\sigma^z\partial_x + i\sigma^x\partial_y)\chi$. Without interactions, ^{3}He-B has a $\mathbb{Z}$ classification; therefore for arbitrary copies of ^{3}He-B, its boundary remains gapless as long as time-reversal symmetry is preserved [12–14]. In other words any fermion-bilinear mass term $\chi_a^\intercal\sigma^y\chi_b$ at the boundary would break the time-reversal symmetry. However, once interactions are turned on, the classification of ^{3}He-B is reduced to $\mathbb{Z}_{16}$; i.e., with 16 copies of ^{3}He-B, its boundary can be gapped out by interactions while preserving the time-reversal symmetry [9,10]. In other words, the boundary is fully gapped by interactions with $\langle\chi_a^\intercal\sigma^y\chi_b\rangle = 0$, for $a,b = 1\cdots16$.

Although the classification of interacting ^{3}He-B has been understood, the following question remains: if the interactions are tuned continuously, can there be a direct second-order quantum phase transition between the weakly interacting gapless boundary and the strongly interacting fully gapped nondegenerate boundary state? Even if such a second-order phase transition exists, its field theory description is unknown because the standard field theory that describes a phase transition of interacting Dirac or Majorana fermions is the Gross-Neveu model [15], which corresponds to the order-disorder phase transition of a bosonic field ϕ_{ab} that couples to a fermion bilinear mass operator: $\phi_{ab}\chi_a^\intercal\sigma^y\chi_b$ [41]. Therefore in the Gross-Neveu model, the gap of the Majorana fermion is induced by a nonzero expectation value of a fermion bilinear mass: $\langle\chi_a^\intercal\sigma^y\chi_b\rangle \neq 0$, which would break the time-reversal symmetry at the boundary of ^{3}He-B.

In this paper we will demonstrate that such a novel direct second-order transition indeed exists, which is fundamentally different from the standard Gross-Neveu theory. But instead of studying the boundary of a $3d$ system (which is numerically challenging), we will just study a $2d$ lattice model, whose low-energy field theory Lagrangian is identical to the boundary of 16 copies of ^{3}He-B, although its fields transform very differently under symmetry groups (the exact boundary field theory of ^{3}He-B cannot be realized in $2d$). We will demonstrate that in this $2d$ lattice model there is indeed a direct second-order quantum phase transition between 16 flavors of gapless $(2+1)d$ Majorana fermions (8 copies of Dirac fermions) and a fully gapped phase that does not break the symmetry of the lattice model. This shows that the fermion gap does not correspond to any fermion bilinear mass.

We will also study another exotic quantum phase transition between the weakly interacting quantum spin Hall (QSH) insulator with spin S^z conservation and spin topological number 2, and the fully gapped and symmetric phase in the strong interaction limit mentioned in the previous paragraph. In the noninteracting limit, the phase transition between the topological insulator and trivial insulator is driven by closing the Dirac mass gap, which requires that the single-particle excitation is gapless at the critical point. However, in this paper we demonstrate that, with interaction, at this quantum phase transition the spin and charge gaps both close, while the single-particle excitation remains gapped. Therefore, this quantum phase transition only involves bosonic degrees of freedom, which allows this quantum phase transition to be described by a bosonic field theory. We propose that the field theory for this transition is an $O(4)$ nonlinear sigma model field theory with a Θ term. The QSH insulator and the trivial phase correspond to $\pi < \Theta \leqslant 2\pi$ and $0 \leqslant \Theta < \pi$, respectively, while the quantum critical point corresponds to $\Theta = \pi$.

II. MODEL HAMILTONIAN

The Hamiltonian we study is an interacting spin-1/2 fermion system defined on a bilayer honeycomb lattice

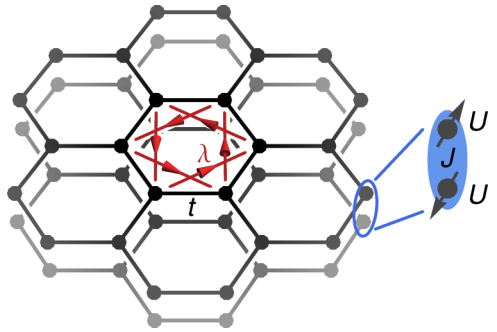

FIG. 1. (Color online) The bilayer honeycomb lattice. In each layer, t and λ are the nearest- and next-nearest-neighbor hopping. The Hubbard interaction U acts on each site, and the Heisenberg interaction J acts across the layers.

(Fig. 1):

$$\begin{aligned} H &= T + T' + W, \\ T &= -t \sum_{\langle ij \rangle} \sum_{\ell,s} (c^\dagger_{i\ell s} c_{j\ell s} + \text{H.c.}), \\ T' &= i\lambda \sum_{\langle\langle ij \rangle\rangle} \sum_{\ell} \nu_{ij} c^\dagger_{i\ell} \sigma^z c_{j\ell}, \\ W &= \frac{U}{2} \sum_{i,\ell} (n_{i\ell} - 1)^2 \\ &\quad + J \sum_i \left[\boldsymbol{S}_{i1} \cdot \boldsymbol{S}_{i2} + \frac{1}{4}(n_{i1} - 1)(n_{i2} - 1) - \frac{1}{4} \right], \end{aligned} \tag{1}$$

where $s = \uparrow, \downarrow$ and $\ell = 1,2$ denote the spin and layer indexes. $T + T'$ corresponds to two layers of the Kane-Mele model [16], and W describes both the on-site and the interlayer interactions. We will set $t = 1$ as the energy unit throughout this paper. We also define $n_{i\ell} = n_{i\ell\uparrow} + n_{i\ell\downarrow}$, $S^\mu_{i\ell} = \frac{1}{2} c^\dagger_{i\ell} \sigma^\mu c_{i\ell}$, and $n_{i\ell s} = c^\dagger_{i\ell s} c_{i\ell s}$. $\langle\langle i, j \rangle\rangle$ stands for a next-nearest-neighbor lattice link. $\nu_{ij} = \pm 1$ depending on whether the hopping path defined by the nearest-neighbor bonds connecting sites i and j bends to the right or to the left. With only the T term, the low-energy limit of this model is described by 8 flavors of $(2+1)d$ massless Dirac fermions (or 16 Majorana fermions) in its Brillouin zone.

In the noninteracting limit, i.e., $U = J = 0$, a nonzero λ will cause the T' term to gap out T and drive the system into a QSH phase with spin topological number $C_s = \pm 2$ which corresponds to the quantized spin Hall conductance $\sigma^{\text{spin}}_H = \frac{e}{2\pi} C_s$. The U term in the Hamiltonian W is a Hubbard repulsion while the J term consists of an antiferromagnetic Heisenberg spin interaction between the two layers and a density-density interaction. In this paper we will fix $J/U = 2$ (with positive U and J). The interaction tends to gap out the charge fluctuations and couples the spins across the layers into the singlet state on each site. Then in the strong interacting limit, the ground state is simply a product state of interlayer spin singlets,

$$|\Psi\rangle = \prod_i (c^\dagger_{i1\uparrow} c^\dagger_{i2\downarrow} - c^\dagger_{i1\downarrow} c^\dagger_{i2\uparrow}) |0\rangle, \tag{2}$$

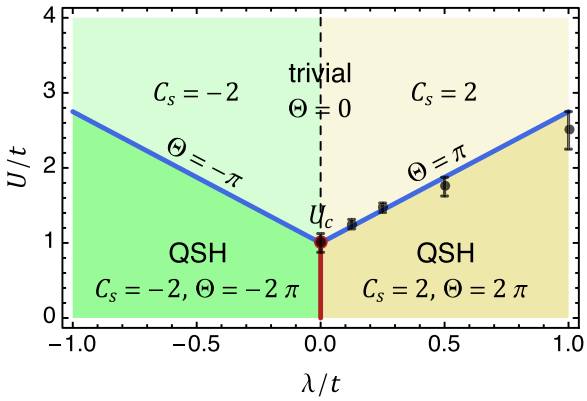

FIG. 2. (Color online) A schematic phase diagram of the bilayer honeycomb model. The red line is the phase boundary between the two QSH phases of opposite spin Hall conductivity, where both the single-particle and the spin/charge gaps are closed. The blue line is the phase boundary between the QSH phase $\Theta = \pm 2\pi$ and the trivial gapped phase $\Theta = 0$, where the single-particle gap remains open but the spin/charge gaps are closed. U_c is the tricritical point, above which the topological number defined in Eq. (6) changes inside the trivial phase (without gap closing) through the dashed line; also see Fig. 3.

which is a trivial gapped state that respects all of the symmetry. Obviously this strongly interacting trivial state should not have any spin Hall responsef; thus it must be separated from the weak interacting QSH states by phase transitions. The phase diagram of this model is depicted in Fig. 2 (see also Fig. 3). Note that the spin topological number C_s shown in the phase diagram is calculated from the single-particle Green's function [to be discussed later in Eq. (6)], and in the strong interacting regime, C_s is no longer related to the spin Hall conductance σ^{spin}_H. In fact, $\sigma^{\text{spin}}_H = 0$ holds for the entire trivial insulating phase despite $C_s = \pm 2$.

It is also worth mentioning that if we fix the ratio $J/U \ll 1$ and increase the interaction gradually, then an intermediate antiferromagnetic (AF) phase could set in between the trivial

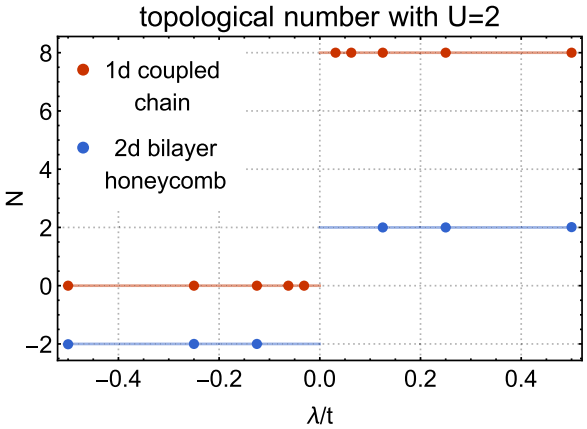

FIG. 3. (Color online) The topological number defined in Eq. (6) as a function of λ for both models at $U = 2$. The topological number was calculated at the dots using determinant QMC data via the methods discussed in Appendix F. This demonstrates that this topological number Eq. (6) is nonzero even in the strongly interacting trivial phase.

phase and the QSH phase, because a nearest-neighbor AF interaction $\sim t^2/U$ could be generated through superexchange. However we will leave this intermediate AF phase for future investigation, and focus on the $J/U = 2$ case where the trivial and the QSH phases are separated by only one single phase transition which turns out to be more exotic.

III. PHASES AND EXCITATION GAPS

Before we present our results for the $2d$ model, we will first consider a $1d$ system composed of two coupled chains. In this $1d$ system, T' becomes

$$T'_{1d} = -\frac{\lambda}{2}\sum_{i,\ell,s}(-)^i(c^\dagger_{i+1,\ell,s}c_{i,\ell,s} + \text{H.c.}). \tag{3}$$

In the noninteracting limit, $\lambda < 0$ corresponds to 4 copies of the Su-Schrieffer-Heeger model of polyacetylene [17] or 8 copies of the Kitaev's $1d$ topological superconductor [42] with a nontrivial boundary state, while $\lambda > 0$ corresponds to a trivial state [3]. We are interested in connecting the $\lambda < 0$ SPT phase to the $\lambda > 0$ trivial phase without a phase transition. (This demonstrates the already known fact that $\lambda < 0$ and $\lambda > 0$ are actually in the same phase under interaction [3].) Fidkowski and Kitaev demonstrated how to do this in one dimension using an interaction term [3] which corresponds to W but with a simpler J term: $+J\boldsymbol{S}_{i,1}\cdot\boldsymbol{S}_{i,2}$. We modify Fidkowski and Kitaev's interaction term slightly so that it can be simulated by quantum Monte Carlo (QMC) without a sign problem [18]. This modification will not change the qualitative results of the model.

Our results are depicted in Figs. 4(a) and 4(b). With $\lambda = 0$, the system is gapped out immediately with infinitesimal interaction, because as was computed explicitly, the four-fermion term is marginally relevant at $\lambda = 0$. The gap we measure scales exponentially with $1/U$, which is consistent with the renormalization group calculation. With finite λ, there is no phase transition at finite U [see Fig. 4(b)]; namely the entire phase diagram of this $1d$ system is one trivially gapped phase except for the isolated gapless point $\lambda = U = J = 0$.

Now let us move on to the honeycomb lattice. It is well known that a weak short-range interaction is irrelevant for a massless $(2+1)d$ Dirac/Majorana fermion, which implies that the interaction can gap out the fermion only when it is strong enough. Thus along the $\lambda = 0$ axis in Fig. 2, a semimetal-insulator phase transition is expected at finite U/t. Indeed, our numerical results suggest that with increasing U/t, there is one continuous phase transition at finite $U_c/t \sim 1$ where the single-particle gap opens up gradually from zero, and the single-particle gap increases monotonically afterwards. In the large U/t limit, this model is exactly soluble, and the ground state is a trivial direct product of on-site spin singlets between the two layers as in Eq. (2). Therefore in the large U/t limit this gapped phase does not correspond to any fermion quadratic mass term. But it is still possible that some other symmetry-breaking order parameters may emerge for intermediate U/t. To verify that this is not the case, we performed a mean-field analysis where we focus on the order parameters that minimize the energy of the interaction term at the mean-field level. The details of this

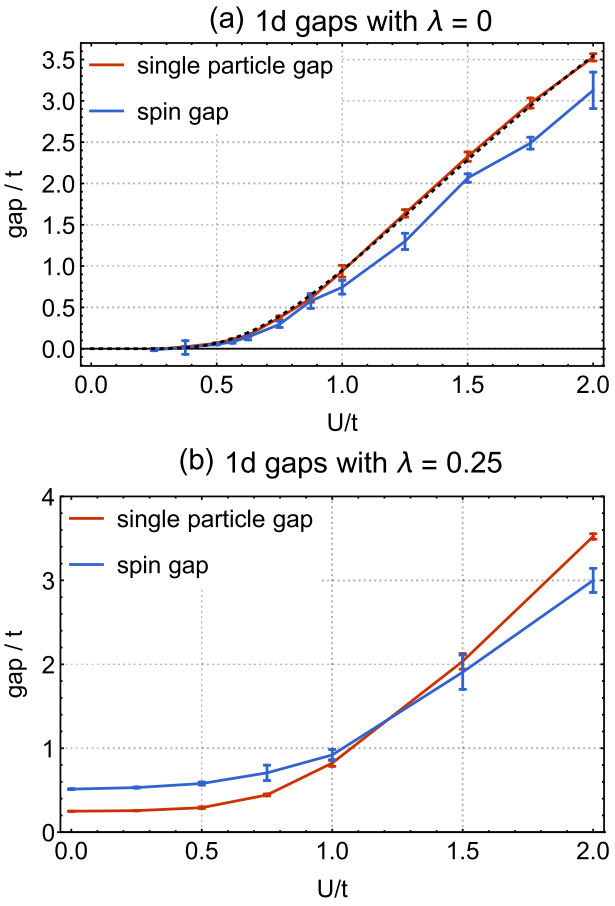

FIG. 4. (Color online) Single particle and spin gap for the $1d$ coupled chain model with $J/U = 2$. (a) When $\lambda = 0$, the system is gapped out immediately by an infinitesimal interaction with a gap of the form $e^{a-b/U}$ for small U (dotted black line with $a = 2.60$ and $b = 2.65$). (b) When $\lambda = 0.25$, there are no phase transitions when $\lambda \neq 0$ and $U > 0$.

mean-field analysis are presented in Appendix A. We identify three order parameters that could potentially minimize the interaction energy: the antiferromagnetic spin density wave (SDW) order, the interlayer spin singlet Cooper pairing, and the interlayer exciton excitation. Among them, the SDW order and the exciton order can be rotated to each other under an SO(5) symmetry emerged at $J = 2U$ point (see Appendix C). So we only need to check the SDW and the pairing orders. Our numerical results suggest that none of these order parameters emerge and stabilize in the entire phase diagram (spin and charge gaps open up continuous from the same critical point as the single-particle gap). Thus we conclude that there can indeed be a continuous quantum phase transition between the gapless Dirac/Majorana fermion phase in the weak interacting limit and the fully gapped symmetric trivial phase in the strong interaction limit.

Since the quantum phase transition is continuous, there must be a field theory description for this phase transition. Furthermore, this field theory must be described by a Lagrangian with 16 flavors of $(2+1)d$ Majorana fermions with four-fermion short-range interactions, but its physics and universality class must be fundamentally different from

the standard Gross-Neveu model. The same field theory Lagrangian must be applicable to the interaction-driven mass gap at the boundary of 16 copies of the ^{3}He-B phase. The only difference is that at the $2d$ boundary of ^{3}He-B a fermion bilinear mass term is prohibited by time-reversal symmetry only, while in our $2d$ lattice model crystalline symmetry is required to prevent fermion bilinear mass terms.

We also note that a similar phase transition between gapless Dirac fermions and a symmetric gapped phase was recently also studied in high energy physics communities [19].

Now let us consider the case with finite λ. In the noninteracting limit, a finite λ term will drive the system into a quantum spin Hall insulator with spin topological number $C_s = 2$; i.e., the Chern number for a spin-up (spin-down) fermion is $+2$ (-2) [see Eq. (6) for definition]. Because our system has S^z conservation, this state is still a nontrivial topological insulator with stable boundary states. While increasing U/t, there must be a quantum phase transition between this topological insulator and the strongly coupled trivial gapped state (blue line in the phase diagram Fig. 2). In the noninteracting limit, the transition between a topological insulator and trivial insulator is driven by closing the Dirac fermion gap. In Fig. 5(b) we can see that there is indeed a quantum phase transition at finite U/t, but at this quantum critical point the single-particle gap does not close, while our data suggest that the gaps for the SDW fluctuation $[\hat{N}^x \sim (-1)^{i+\ell} c^\dagger_{i,\ell}\sigma^x c_{i,\ell}$, $\hat{N}^y \sim (-1)^{i+\ell} c^\dagger_{i,\ell}\sigma^y c_{i,\ell}]$ and the pairing fluctuation $(\hat{\Delta} \sim c^{\mathsf{T}}_{i,1} i\sigma^y c_{i,2})$ (referred to as the spin and the charge gaps, respectively) both vanish at the critical point. A similar unconventional phase transition was also found in $1d$ systems in Ref. [20], where the gaps also closed in the collective spin/charge excitations rather than in the single-particle excitations. This implies that in the low-energy limit this quantum phase transition only involves bosonic degrees of freedom, allowing the fermionic excitations to be integrated out from the field theory.

Close to the quantum critical point, we can define a four-component unit vector $\boldsymbol{n}$ with $\boldsymbol{n}^2 = 1$, which couples to the fermions as follows:

$$n_1\hat{N}^x + n_2\hat{N}^y + n_3\mathrm{Re}(\hat{\Delta}) + n_4\mathrm{Im}(\hat{\Delta}). \tag{4}$$

We propose that the phase diagram for $\lambda \neq 0$ can be described by the following effective bosonic field theory:

$$S = \int d^2x d\tau \, \frac{1}{g}(\partial_\mu \boldsymbol{n})^2 + \frac{i\Theta}{\Omega_3}\epsilon_{abcd} n^a \partial_x n^b \partial_y n^c \partial_\tau n^d, \tag{5}$$

where $\Omega_3 = 2\pi^2$ is the volume of a three-dimensional sphere with unit radius. The field theory Eq. (5) can be derived using the same method as Ref. [21], after integrating out the fermions. The phase diagram and renormalization group flow of the $(1+1)d$ analog of Eq. (5) were calculated explicitly in Refs. [22–24], and it was demonstrated that the entire phase $0 \leqslant \Theta < \pi$ is controlled by the fixed point $\Theta = 0$, while the entire phase $\pi < \Theta \leqslant 2\pi$ will flow to the fixed point $\Theta = 2\pi$. $\Theta = \pi$ is the phase transition between the two phases. The phase diagram of Eq. (5) was studied in Ref. [25], and again in the disordered phases (phases with large g) $\Theta = \pi$ is the quantum phase transition between the two phases with $0 \leqslant \Theta < \pi$ and $\pi < \Theta \leqslant 2\pi$.

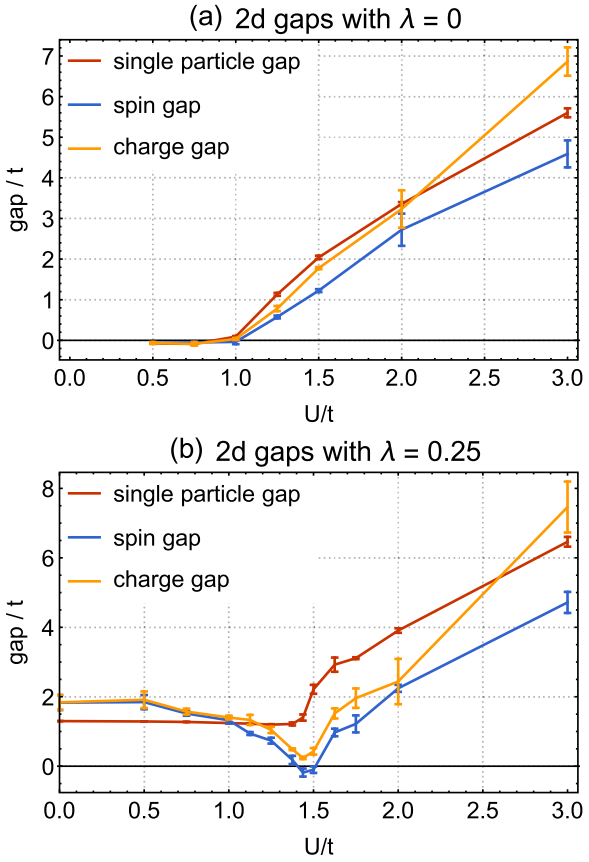

FIG. 5. (Color online) Single-particle gap, spin gap (gap for spin-1 excitation), and charge gap (gap for charge-2 excitation) on the bilayer honeycomb lattice with $J/U = 2$. (a) When $\lambda = 0$, there is a single continuous phase transition from a semimetal to a trivial insulator at $U_c \sim 1$, whose field theory also describes the phase transition of the boundary of 16 copies of the ^{3}He-B phase. (b) When $\lambda = 0.25$, only the spin and charge gap close at the continuous phase transition from an SPT to a trivial insulator (which is at $U_c \sim 1.5$ for $\lambda = 0.25$). We propose that this phase transition is described by a bosonic $O(4)$ nonlinear sigma model field theory with a Θ term [Eq. (5)]. These gaps are calculated as explained in Appendix E. This involves calculating gaps in finite systems of sizes up to 9×9 unit cells (with 4 sites each) and extrapolating to the infinite-size limit. Error bars on all figures denote one standard deviation (i.e., ≈68% confidence).

In Eq. (5), the fixed point $\Theta = 2\pi$ describes a bosonic symmetry-protected topological (SPT) state with $U(1) \times U(1)$ symmetry [26], where the two $U(1)$ symmetries correspond to charge and S^z conservation, respectively. The boundary of Eq. (5) with $\Theta = 2\pi$ is a $(1+1)d$ $O(4)$ nonlinear sigma model with a Wess-Zumino-Witten term at level $k = 1$, which corresponds to a $(1+1)d$ conformal field theory. In the bulk theory we can define two bosonic rotor fields $b_1 \sim n_1 + in_2$ and $b_2 \sim n_3 + in_4$. b_1 and b_2 carry spin-1 and charge-2, respectively. The fixed point $\Theta = 2\pi$ in Eq. (5) implies that a vortex of (n_3,n_4)(2π vortex of b_2, also π flux seen by the fermions) carries one b_1 boson; namely a π flux for fermions carries spin $S^z = 1$, which is precisely consistent with the QSH insulator with spin topological number 2 [27,28]. Thus the fixed point $\Theta = 2\pi$ has all the key properties of the QSH

insulator phase. At the fixed point $\Theta = 0$, the boundary of Eq. (5) is trivial. The phase transition between the quantum spin Hall insulator and the trivial state can be driven by tuning the parameter Θ, where the quantum critical point corresponds to $\Theta = \pi$.

IV. SPIN TOPOLOGICAL NUMBER AND GREEN'S FUNCTION

Having mapped out the phase boundaries in the phase diagram, let us discuss the topological properties of the various phases. The gapped ground states of the bilayer honeycomb model in Eq. (1) belong to the fermion SPT phases protected by both the charge and the spin $U(1)$ symmetries, which is $\mathbb{Z}$ classified (even with interaction). With this classification, each SPT state is characterized by a quantized topological number, the spin Chern number, in analogy to the TKNN integer for integer quantum Hall states, which can be constructed by the following fermion Green's function [29–36] as

$$C_s = \frac{1}{48\pi^2}\int d^3k\epsilon^{\mu\nu\lambda}\mathrm{Tr}[-\sigma^z G\partial_\mu G^{-1} G\partial_\nu G^{-1} G\partial_\lambda G^{-1}], \tag{6}$$

where σ^z is the spin S^z matrix, $G(k) = -\langle c_k c_k^\dagger\rangle$ is the fermion Green's function in the frequency and momentum space $k = (i\omega, \boldsymbol{k})$ with $i\omega$ being the Matsubara frequency, and ∂_μ here stands for $\partial/\partial k_\mu$. In the noninteracting limit, the physical meaning of the topological number Eq. (6) is associated with the spin Hall conductance $\sigma_H^{\mathrm{spin}} = C_s e/2\pi$. Nevertheless, the formula Eq. (6) is still well defined for interacting systems, as long as we use the full interacting fermion Green's function [29,30,33–36]. However, for interacting systems, this topological number defined with full Green's function no longer necessarily corresponds to the spin Hall response.

In the weak interaction regime, the spin topological number for the bilayer QSH state is $C_s = \pm 2$, depending on the sign of λ. The two QSH phases are separated by a topological phase transition at $\lambda = 0$ (the red line in Fig. 2), where the single-particle gap closes, and the Green's function develops poles at zero frequency and at the K and K' points in the Brillouin zone. Due to this singularity of the Green's function, the spin topological number is allowed to change across the gapless phase boundary. Above the critical point U_c, this phase transition is gapped out by interaction, but the topological number Eq. (6) still changes discontinuously across $\lambda = 0$, as proven in Ref. [37]. The transition of the topological number (dashed violet line in Fig. 2) hidden in the trivial gapped phase implies that the Green's function must have zeros (instead of poles) at zero frequency. This is based on the observation that in Eq. (6) G and G^{-1} are interchangeable, so the topological number can either change through the poles of G or the zeros of G (which are poles of G^{-1}) [20,37]. When the fermions are gapped out by strong interaction, it is impossible to have poles of G at zero frequency, so the topological number Eq. (6) can only change through the zeros of G.

The zeros of the Green's function are a prominent property of the trivial gapped phase ($U > U_c$), in contrast to the poles along the topological phase boundary ($U < U_c$). It is found that both the poles and the zeros are located at the K and K' points in the Brillouin zone, and can be verified in our QMC simulation. Along the $\lambda = 0$ axis, the Green's function at the K point $G(\omega, K)$ develops a pole as $\omega \to 0$ when $U < U_c$ [Fig. 6(a)], while it approaches zero when $U > U_c$ [Fig. 6(b)]. In the strong interaction limit, Ref. [37] predicts that the Green's function should follow the behavior $G(\omega, K) \simeq \omega/(\omega^2 + \Delta^2)$ (where $\Delta \sim U$ is the typical scale of the quasiparticle gap), and in the zero-frequency limit $G(\omega, K) \propto \omega$ approaches to zero linearly with ω. Our numerical result matches all these predictions quite well.

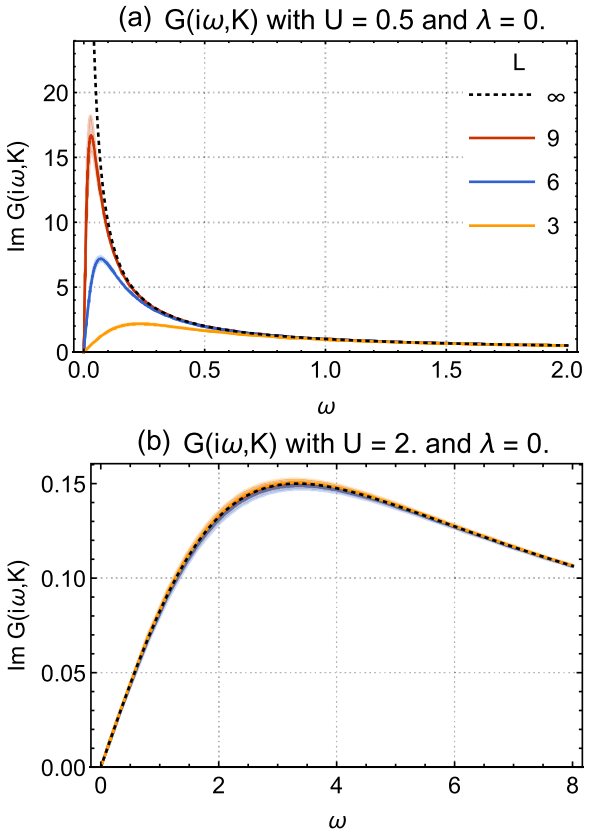

FIG. 6. (Color online) Green's function $G(i\omega, K)$ as a function of frequency at the K point with $\lambda = 0$ and $J/U = 2$ on the bilayer honeycomb lattice for various system sizes. [The largest eigenvalue of $G(i\omega = 0, K)$ is shown.] (a) In the free fermion limit when $U \ll U_c \sim 1.5$, the Green's function shows a pole at zero frequency: $G(i\omega, K) \simeq 1/(i\omega)$ [Eq. (B2)] (dotted black line). (b) In the strong interacting limit when $U \gg U_c \sim 1.5$, the Green's function follows the behavior of $G(i\omega, K) \simeq (i\omega)/[(i\omega)^2 - \Delta^2]$ [as calculated in Eq. (B3)] (dotted black line) where Δ is the quasiparticle gap. Please note that here ImG is the imaginary part of the imaginary-time Green's function, which is very different from the spectral function.

V. SUMMARY

In this work we demonstrate that there exist two novel continuous quantum phase transitions for 16 copies of $(2+1)d$ Majorana fermions; both cases are very different from the Standard Gross-Neveu model and Ginzburg-Landau theory. However, a controlled analytical field theory calculation for

the critical exponents is not known yet; we will leave this to future studies.

ACKNOWLEDGMENTS

We acknowledge support from the Center for Scientific Computing at the CNSI and MRL: an NSF MRSEC (DMR-1121053) and NSF CNS-0960316. The authors are supported by the the David and Lucile Packard Foundation and NSF Grant No. DMR-1151208.

APPENDIX A: MEAN-FIELD ENERGY OF ORDER PARAMETERS

In this appendix, we will investigate the order parameters that are favored at the mean-field level. Since our model only has on-site interactions, we will only consider on-site order parameters in this appendix.

We start from the free fermion limit. In momentum space, the fermion kinetic Hamiltonian takes the form

$$T+T'=\sum_{\boldsymbol{k}}\sum_{\ell=1,2}[c^\dagger_{\boldsymbol{k}A\ell}\ \ c^\dagger_{\boldsymbol{k}B\ell}]\begin{bmatrix} g(\boldsymbol{k})\sigma^z & f^*(\boldsymbol{k})\\ f(\boldsymbol{k}) & -g(\boldsymbol{k})\sigma^z\end{bmatrix}\begin{bmatrix}c_{\boldsymbol{k}A\ell}\\ c_{\boldsymbol{k}B\ell}\end{bmatrix}, \tag{A1}$$

where A and B label the sublattice sites in each unit cell, $g(\boldsymbol{k})=-2\lambda\big(\sin\sqrt{3}k_x-2\sin\frac{\sqrt{3}k_x}{2}\cos\frac{3k_y}{2}\big)$, and $f(\boldsymbol{k})=-t\big(e^{-ik_y}+2e^{ik_y/2}\cos\frac{\sqrt{3}k_x}{2}\big)$. Let us first switch to the Majorana fermion basis

$$\chi_{\boldsymbol{k}}=\underbrace{\begin{bmatrix}K\\K'\end{bmatrix}}_{\text{valley}}\otimes\underbrace{\begin{bmatrix}A\\B\end{bmatrix}}_{\text{sublattice}}\otimes\underbrace{\begin{bmatrix}1\\2\end{bmatrix}}_{\text{layer}}\otimes\underbrace{\begin{bmatrix}\uparrow\\\downarrow\end{bmatrix}}_{\text{spin}}\otimes\underbrace{\begin{bmatrix}\mathrm{Re}\,c_{\boldsymbol{k}}\\ \mathrm{Im}\,c_{\boldsymbol{k}}\end{bmatrix}}_{\text{particle-hole}}, \tag{A2}$$

then expand the kinetic Hamiltonian $T+T'$ around the $K=(+\frac{4\pi}{3\sqrt{3}},0)$ and $K'=(-\frac{4\pi}{3\sqrt{3}},0)$ points in the Brillouin zone,

$$T+T'=\frac{1}{2}\sum_{\boldsymbol{k}}\chi^\intercal_{-\boldsymbol{k}}(vk_x\sigma^{31000}+vk_y\sigma^{02002}+m\sigma^{33032})\chi_{\boldsymbol{k}}, \tag{A3}$$

where $\sigma^{ijk\cdots}\equiv\sigma^i\otimes\sigma^j\otimes\sigma^k\otimes\cdots$ stands for the direct product of Pauli matrices, $v=3t/2$, and $m=3\sqrt{3}\lambda$. We consider all the fermion bilinear orders $\Delta^{v\alpha\ell\sigma\psi}=\chi^\intercal\sigma^{v\alpha\ell\sigma\psi}\chi$ that can gap out the fermions at the K and K' points to gain a kinetic energy benefit, implying that $\sigma^{v\alpha\ell\sigma\psi}$ must be a 32×32 antisymmetric matrix that anticommutes with both σ^{31000} and σ^{02002}. We found 136 such matrices that are qualified as the fermion mass terms.

Next we consider the interaction effect. Among the 136 potential orders, the interaction W will select out the most favorable ones. To determine the most favorable orders, we calculate the mean-field (Hartree-Fock) energy of W for the potential orders $\Delta^{v\alpha\ell\sigma\psi}$, such that the interaction term decomposes into that ordering channel as $W=w_{v\alpha\ell\sigma\psi}|\Delta^{v\alpha\ell\sigma\psi}|^2$ with the mean-field energy $w_{v\alpha\ell\sigma\psi}$. The orders that can gain an interaction energy benefit (i.e., $w_{v\alpha\ell\sigma\psi}<0$ given $U,J>0$) are concluded in Table I: the layer-antiferromagnetic spin density wave, the interlayer exciton order, and the interlayer spin-singlet pairing order. When $\lambda\neq0$, the λ term suppresses the exciton order and the z component of the spin density wave. As a result, when $\lambda\neq0$ we only consider the XY component of the Néel order and the pairing order, which exactly corresponds to the four-component vector $\boldsymbol{n}$ defined in Eq. (4).

TABLE I. Mean-field energy of the interaction favored fermion bilinear orders. When $J/U=2$, there is an SO(5) symmetry [Eq. (C3)] which mixes the spin density wave and exciton order parameters so that these order parameters transform like a vector with $n=(\Delta^{03312},\Delta^{03320},\Delta^{03332},\Delta^{03200},\Delta^{03102})$. The degeneracy of the mean-field energies of the exciton order and the pairing order is not associated with a symmetry.

$w_{v\alpha\ell\sigma\psi}$	$\Delta^{v\alpha\ell\sigma\psi}$	Physical meaning
$-(J+2U)/4$	Δ^{03312} Δ^{03320} Δ^{03332}	layer-antiferromagnetic s-wave spin density wave
$-J/2$	Δ^{03102} Δ^{03200}	interlayer s-wave exciton order
$-J/2$	Δ^{10121} Δ^{10123}	interlayer spin-singlet s-wave superconductivity

APPENDIX B: GREEN'S FUNCTION IN BOTH FREE AND STRONG INTERACTING LIMITS

In this appendix, we will calculate the fermion Green's function analytically in both the free and the strong interacting limits. Suppose that in the Majorana basis, the kinetic Hamiltonian takes the most general fermion bilinear form $T+T'=\sum_{a,b}iu_{ab}\chi_a\chi_b$, where a and b are the combined label of site, layer, spin, and particle-hole indices, and χ_a and χ_b are the corresponding Majorana fermion operators. The full Hamiltonian $H=T+T'+W$ also includes the interaction term $W=\sum_i\sum_{[\alpha_k]}w_{\alpha_1\alpha_2\alpha_3\alpha_4}\chi_{i\alpha_1}\chi_{i\alpha_2}\chi_{i\alpha_3}\chi_{i\alpha_4}$, where i labels the site and α_k labels the rest of the internal degrees of freedoms.

Consider the fermion Green's function, which is defined as $G_{ab}=-\langle\chi_a\chi_b\rangle$. In the free fermion limit, the Green's function can be simply obtained from the single-particle Hamiltonian via $(G^{-1})_{ab}=i\omega\delta_{ab}-iu_{ab}$. In momentum space (expanded around the K and K' points) and using the Majorana basis, the kinetic Hamiltonian reads (see the previous appendix)

$$T+T'=\frac{1}{2}\sum_{\boldsymbol{k}}\chi^\intercal_{-\boldsymbol{k}}(vk_x\sigma^{31000}+vk_y\sigma^{02002}+m\sigma^{33032})\chi_{\boldsymbol{k}}. \tag{B1}$$

So in the free fermion limit, the Green's function is

$$\begin{aligned}G(i\omega,\boldsymbol{k})&=(i\omega\sigma^{00000}-vk_x\sigma^{31000}-vk_y\sigma^{02002}-m\sigma^{33032})^{-1}\\&=\frac{i\omega\sigma^{00000}+vk_x\sigma^{31000}+vk_y\sigma^{02002}+m\sigma^{33032}}{(i\omega)^2-(v^2\boldsymbol{k}^2+m^2)},\end{aligned} \tag{B2}$$

where $v = 3t/2$ and $m = 3\sqrt{3}\lambda$ are determined by the hopping parameters. While in the strong interacting limit, the Green's function (at low-frequency limit) has the form

$$G(i\omega,\boldsymbol{k}) \simeq \frac{i\omega\sigma^{00000} + \sum_{n=0}^{\infty} g_n (vk_x\sigma^{31000} + vk_y\sigma^{02002} + m\sigma^{33032})^{2n+1}}{(i\omega)^2 - \Delta^2} + O(\omega^2)$$
$$= \frac{i\omega\sigma^{00000} + \sum_{n=0}^{\infty} g_n (v^2\boldsymbol{k}^2 + m^2)^n (vk_x\sigma^{31000} + vk_y\sigma^{02002} + m\sigma^{33032})}{(i\omega)^2 - \Delta^2} + O(\omega^2), \quad \text{(B3)}$$

where g_n are coefficients and the single-particle gap $\Delta = U/2 + 3J/4$ is determined by the interaction parameters. In our QMC simulation, we set $J = 2U$, so $\Delta = 2U$ in the $U \to \infty$ limit. However for finite U in our simulation, the single-particle gap Δ should generally be softer ($\Delta < 2U$). As one can see, Eq. (B3) has the same structure on the numerator as Eq. (B2), so they should result in the same topological number. It is also found that $g_0 = 0$ for our model; however, this does not affect the topological number.

At the K (or K') point, we set $\boldsymbol{k} = 0$. Thus from the above results, we conclude that along the $\lambda = 0$ axis (such that $m = 0$) and below $U_c \sim 1.5$, the Green's function shows a pole at zero frequency: $G(i\omega, K) \simeq 1/(i\omega)$ [Fig. 6(a)], while above U_c, the Green's function follows the behavior of $G(i\omega, K) \simeq (i\omega)/[(i\omega)^2 - \Delta^2]$ [Fig. 6(b)], where Δ is the quasiparticle gap. Away from the $\lambda = 0$ axis and at zero frequency, the Green's function is expected to decay as $1/\lambda$ (Fig. 7) in the free fermion limit. Our numerical results are perfectly consistent with the predictions made above (see Figs. 6 and 7).

APPENDIX C: CONTINUOUS SYMMETRIES

In this appendix we study the continuous symmetries of our $2d$ model, which allow us to simplify our analysis. A summary is given in Table II. The symmetries of our model are easiest to understand in a Majorana basis, which was introduced in Appendix A. In the exciton channel, interaction W_i takes the form

$$W_i = 2^{-6} \sum_{\alpha=0,3} \sum_{\ell=0}^{3} \sum_{\psi=0,2} \times \begin{cases} +U, & \ell = 0,3, \\ -J/2, & \ell = 1,2, \end{cases} \left(\chi_i^T \sigma^{\alpha\ell 0\psi} \chi_i\right)^2 + \text{const.} \quad \text{(C1)}$$

Here there is no valley index on $\chi_{i\alpha\ell\sigma\psi}$ since χ_i is written is real space:

$$\chi_i = \underset{\text{sublattice}}{\begin{bmatrix} A \\ B \end{bmatrix}} \otimes \underset{\text{layer}}{\begin{bmatrix} 1 \\ 2 \end{bmatrix}} \otimes \underset{\text{spin}}{\begin{bmatrix} \uparrow \\ \downarrow \end{bmatrix}} \otimes \underset{\text{particle-hole}}{\begin{bmatrix} \text{Re}\, c_i \\ \text{Im}\, c_i \end{bmatrix}}. \quad \text{(C2)}$$

When $J/U = 2$ and $\lambda = 0$, this model has a $U(1) \times \text{SO}(5)$ symmetry generated by operators of the form $\sum_i \frac{1}{8}\chi_i^T \Gamma \chi_i$. The $U(1)$ charge symmetry is generated by $\Gamma = \sigma^{0002}$ while the SO(5) symmetry is generated by Γ_{ab}, where

$$\Gamma_{ab} = \begin{bmatrix} 0 & -\sigma^{0032} & +\sigma^{0020} & -\sigma^{0112} & -\sigma^{0210} \\ +\sigma^{0032} & 0 & -\sigma^{0012} & -\sigma^{0120} & -\sigma^{0222} \\ -\sigma^{0020} & +\sigma^{0012} & 0 & -\sigma^{0132} & -\sigma^{0230} \\ +\sigma^{0112} & +\sigma^{0120} & +\sigma^{0132} & 0 & -\sigma^{0302} \\ +\sigma^{0210} & +\sigma^{0222} & +\sigma^{0230} & +\sigma^{0302} & 0 \end{bmatrix}. \quad \text{(C3)}$$

The σ^{0302} matrix corresponds to the conservation of charge on one layer minus the charge on the other layer. σ^{0012}, σ^{0020}, and σ^{0032} correspond to spin rotation symmetry. The other six matrices will mix the spin density wave and exciton order parameters (Table I) so that these order parameters transform like a vector under the above SO(5) symmetry with $n = (\Delta^{03312}, \Delta^{03320}, \Delta^{03332}, \Delta^{03200}, \Delta^{03102})$. If $J/U = 2$ but $\lambda \neq 0$ then symmetry is reduced to $U(1)^2 \times \text{SU}(2)$. The $U(1)$ symmetries are charge conservation and spin rotation about the z axis. The SU(2) symmetry is generated by $\Gamma_a = \sigma^{0132}, \sigma^{0230}, \sigma^{0302}$ (which will mix the S^z spin density

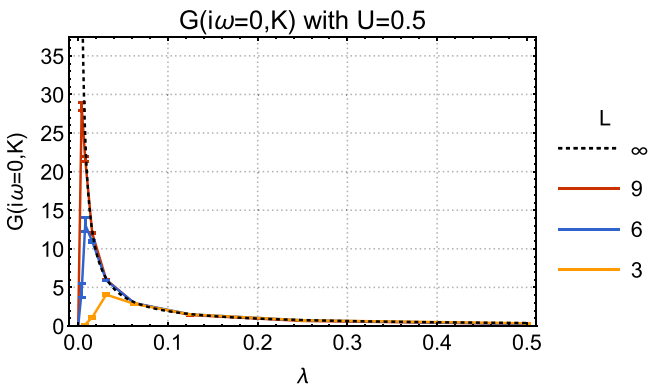

FIG. 7. (Color online) Zero-frequency Green's function $G(i\omega = 0, K)$ at the K point with $J/U = 2$ on the bilayer honeycomb lattice for various system sizes. [The largest eigenvalue of $G(i\omega = 0, K)$ is shown.] In the free fermion limit when $U \ll U_c \sim 1.5$, the Green's function decays as $G(i\omega = 0, K) \simeq 1/3\sqrt{3}\lambda$ [cf. Eq. (B2)] (dotted black line).

TABLE II. A summary of the symmetries of our model for various coupling constants.

Coupling constants	Symmetry
$J/U = 2, \lambda = 0$	$U(1)_{\text{charge}} \times \text{SO}(5)_{\text{layer charge, SDW} \leftrightarrow \text{ exciton, spin}}$
$J/U = 2, \lambda \neq 0$	$U(1)_{\text{charge}} \times \text{SU}(2)_{\text{layer charge, z-SDW} \leftrightarrow \text{exciton}} \times U(1)_{\text{z-spin}}$
$J/U \neq 2, \lambda = 0$	$U(1)_{\text{charge}} \times U(1)_{\text{layercharge}} \times \text{SU}(2)_{\text{spin}}$
$J/U \neq 2, \lambda \neq 0$	$U(1)_{\text{charge}} \times U(1)_{\text{layercharge}} \times U(1)_{\text{z-spin}}$

wave and exciton order parameters and conserve the charge difference between layers).

When $J/U \neq 2$ and $\lambda = 0$ the symmetry is $U(1)^2 \times \mathrm{SU}(2)$, which corresponds to separate $U(1)$ charge conservation on each layer and SU(2) spin rotation. If $J/U \neq 2$ and $\lambda \neq 0$ then the SU(2) spin rotation symmetry reduces to a $U(1)$ spin rotation symmetry about the z axis.

APPENDIX D: QMC METHODS

The numerical results presented in this paper were calculated using projector quantum Monte Carlo (QMC), which is described in detail in Ref. [38]. Projector QMC is a kind of determinant QMC which focuses on the zero-temperature ground states of nondegenerate fermion systems. Determinant QMC is a kind of auxiliary field QMC which uses a (usually discrete) Hubbard-Stratonovich transformation to decouple an interacting fermion Hamiltonian into a noninteracting Hamiltonian. All of these QMC methods are unbiased, controlled, and numerically exact numerical methods to calculate expectation values to arbitrary precision. Ground state expectation values are calculated from the imaginary time evolution of a trial wave function $|\Psi_T\rangle$

$$\langle A\rangle = \lim_{\Theta\to\infty} \frac{\langle\Psi_T|e^{-\Theta H/2}Ae^{-\Theta H/2}|\Psi_T\rangle}{\langle\Psi_T|e^{-\Theta H}|\Psi_T\rangle}; \qquad \text{(D1)}$$

Θ is a projection parameter which projects the trial wave function into the ground state. In practice, one must use a finite but large value for Θ. We chose to use $\Theta = 64/t$ (where t is the hopping strength), which we found to be sufficient. As is typically done, we chose $|\Psi_T\rangle$ to be a Slater determinant in the ground state subspace of the noninteracting part of our interacting Hamiltonian [$T + T'$ from Eq. (1)].

A Trotter decomposition is then applied to the numerator of Eq. (D1) to separate the exponents into three parts:

$$e^{-\Theta H/2} = [e^{-\Delta_\tau(T+T')}e^{-\Delta_\tau H_U}e^{-\Delta_\tau H_J}]^{N_\tau} + O(\Delta_\tau)^2,$$

where $\Delta_\tau = \Theta/2N_\tau$, H_U is the U term of H, and H_J is the J term of H [Eq. (1)]. In our simulations we used $N_\tau \approx \Theta\sqrt{N_{\text{sweeps}}}$ so that the systematic errors due to the Trotter decomposition remain negligible compared to the statistical error resulting from the finite number of Monte Carlo sweeps performed: N_{sweeps}. A sweep has occurred after all field variables have been given the chance to update. We used between 64 and 4096 sweeps for the results shown here. All observables have been checked against exact diagonalization simulations on small lattices. The statistical error due to the finite number of sweeps is shown on all plots as error bars which denote one standard deviation (i.e., ≈68% confidence). A Hubbard-Stratonovich transformation is then applied to the interacting fermion problem to transform it into a free fermion problem at the expense of adding (discrete) bosonic variables. We used the same Hubbard-Stratonovich as introduced in [18]. The imaginary numbers due to the Kane-Mele λ term are dealt with as described in [39].

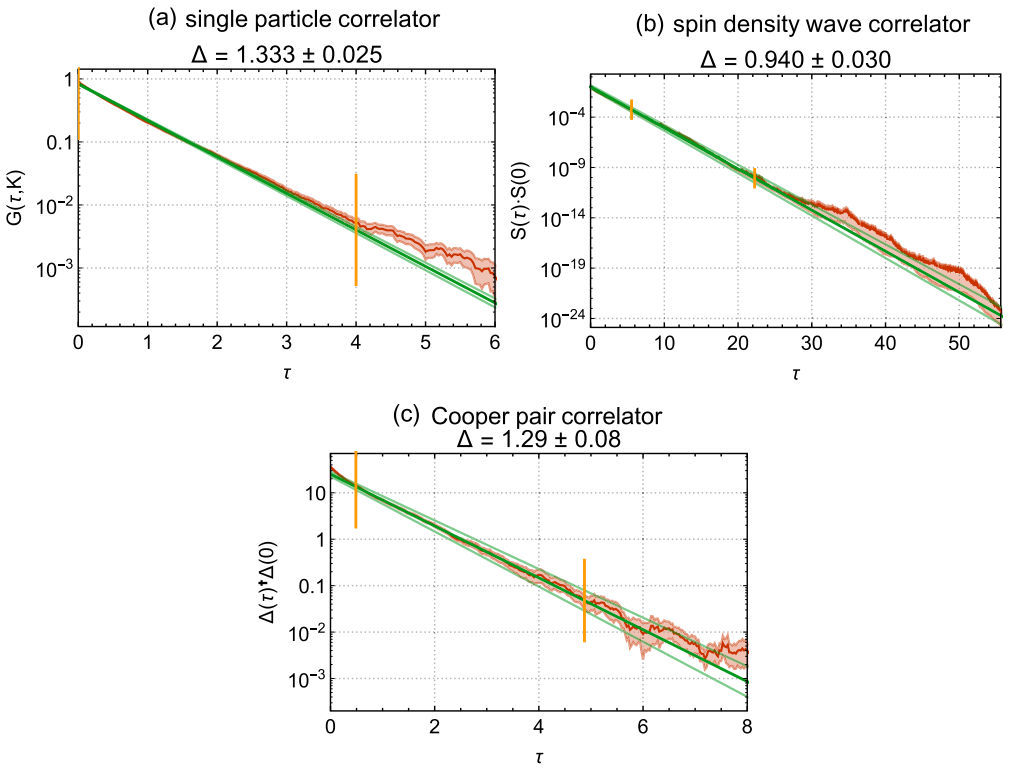

FIG. 8. (Color online) The exponential decay in imaginary time of correlation functions (red line) for various order parameters (Table I) on a honeycomb lattice of dimension 3×3 with $U = 1.4375$, which is nearly at the critical point. The shaded red region denotes statistical errors. The thick green line indicates the fit to $e^{-\tau\Delta+c}$ while the two thin green lines denote the uncertainty of the fit. The fit was performed in the region between the vertical orange lines. The negative of the slope of the fit is the energy gap for the finite-size system, which is used to make Fig. 9.

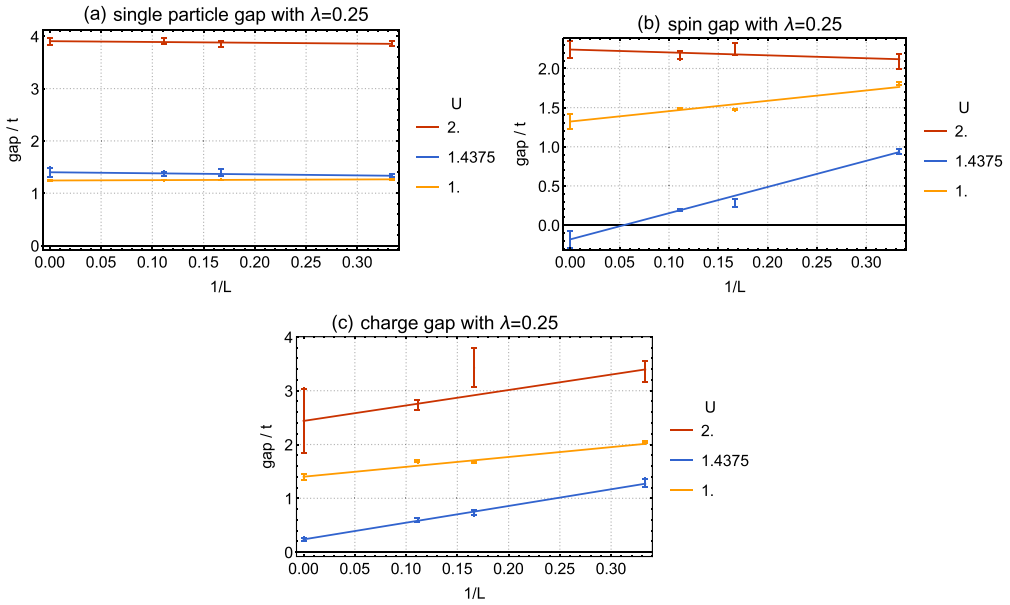

FIG. 9. (Color online) We extrapolate the gaps associated with a single particle (a), spin (b), and charge (c) (Table I) from a system of finite spatial size to one of infinite size. Extrapolations are shown for $\lambda = 0.25$ and interaction strengths below ($U = 1$), near ($U = 1.4375$), and above ($U = 2$) the gapless critical point at $U \sim 1.5$. The results of these extrapolations are used to make Fig. 5(b) ($\lambda = 0.25$ and $J/U = 2$).

APPENDIX E: GAP CALCULATION METHODS

In this appendix we discuss in more detail how the gaps in Figs. 4 and 5 are calculated. (We use the same approach that was used in Ref. [40].) First, we measure the rate of exponential decay in imaginary time of correlation functions for various order parameters (Fig. 8). (QMC is very efficient at making this measurement.) This decay has the form $\langle Q^\dagger Q\rangle \sim e^{-\tau\Delta+c}$ for large separations in imaginary time (i.e., $\tau \gg \Delta^{-1}$) where Δ is the energy gap associated with the order parameter Q. We then extrapolate the finite system size gaps Δ to the gap for a system with infinite size (Fig. 9).

APPENDIX F: TOPOLOGICAL NUMBER CALCULATION METHODS

In this appendix we describe how the topological numbers displayed in Fig. 3 are calculated from the Green's function. In one dimension, the topological number can be written as

$$N = \frac{1}{2\pi i}\int dk\,\mathrm{Tr}[\Sigma G\partial_k G^{-1}], \tag{F1}$$

where $G = G(i\omega = 0,k)$ is the zero-frequency Green's function and $\Sigma = \sigma^{300}$ in the basis

$$c_i = \underbrace{\begin{bmatrix}A\\B\end{bmatrix}}_{\text{sublattice}} \otimes \underbrace{\begin{bmatrix}1\\2\end{bmatrix}}_{\text{layer}} \otimes \underbrace{\begin{bmatrix}\uparrow\\\downarrow\end{bmatrix}}_{\text{spin}}. \tag{F2}$$

To calculate this number using determinant QMC, we first measure the zero-frequency Green's function $G(i\omega = 0)_k$ at the discrete (due to the finite lattice) momenta k. We then promote $G(i\omega = 0)_k$ to a continuous function $G(i\omega = 0,k)$ via interpolation. For example, one could choose a linear interpolation

$$G(i\omega = 0,k) = \frac{k_2 - k}{k_2 - k_1}G(i\omega = 0)_{k_1} + \frac{k - k_1}{k_2 - k_1}G(i\omega = 0)_{k_2}, \tag{F3}$$

where k_1 and k_2 are the nearest discrete momenta to the continuous momentum k. The choice of interpolation method will not affect the topological number as long as the the lattice is large enough to sample enough momenta. This is because N is a topological number and therefore insensitive to local perturbations. (Imagine calculating the winding number of a circle around the origin by approximating the circle as a polygon.) Once $G(i\omega = 0,k)$ has been attained via interpolation, it can be inserted into the equation for N [Eq. (F1)] to attain the topological number via numerical integration.

In two dimensions, the topological number can be written as

$$C_s = \frac{1}{48\pi^2}\int d\omega d^2k\,\epsilon^{\mu\nu\rho}\mathrm{Tr}[\Sigma G\partial_\mu G^{-1}G\partial_\nu G^{-1}G\partial_\rho G^{-1}], \tag{F4}$$

where $G = G(i\omega,k)$ is the Green's function and $\Sigma = -\sigma^{003}$ in the same basis as above. Now, we measure $G_{i\omega,k}$ at discrete Matsubara frequency ω and discrete momenta k and then interpolate it to $G(i\omega,k)$. However, the measured $G_{i\omega,k}$ is only reliable up to $\omega \sim 2\pi N_\tau/\Theta$. Since $G(i\omega,k)$ is expected to approach zero for large ω, we choose to let our interpolation approach zero at a finite $\omega \sim 2\pi N_\tau/\Theta$ and remain at zero for larger ω. Again, this will not affect the calculated topological number as long as N_τ/Θ is sufficiently large. Finally, $G(i\omega,k)$ is inserted into the equation for C_s [Eq. (F4)] using numerical integration.

[1] X. Chen, Z.-C. Gu, Z.-X. Liu, and X.-G. Wen, Phys. Rev. B **87**, 155114 (2013).

[2] X. Chen, Z.-C. Gu, Z.-X. Liu, and X.-G. Wen, Science **338**, 1604 (2012).

[3] L. Fidkowski and A. Kitaev, Phys. Rev. B **81**, 134509 (2010).

[4] L. Fidkowski and A. Kitaev, Phys. Rev. B **83**, 075103 (2011).

[5] X.-L. Qi, New J. Phys. **15**, 065002 (2013).

[6] H. Yao and S. Ryu, Phys. Rev. B **88**, 064507 (2013).

[7] Z.-C. Gu and M. Levin, Phys. Rev. B **89**, 201113(R) (2014).

[8] S. Ryu and S.-C. Zhang, Phys. Rev. B **85**, 245132 (2012).

[9] C. Wang and T. Senthil, Phys. Rev. B **89**, 195124 (2014).

[10] L. Fidkowski, X. Chen, and A. Vishwanath, Phys. Rev. X **3**, 041016 (2013).

[11] Y.-Z. You and C. Xu, Phys. Rev. B **90**, 245120 (2014).

[12] A. P. Schnyder, S. Ryu, A. Furusaki, and A. W. W. Ludwig, AIP Conf. Proc. **1134**, 10 (2009).

[13] S. Ryu, A. Schnyder, A. Furusaki, and A. Ludwig, New J. Phys. **12**, 065010 (2010).

[14] A. Y. Kitaev, AIP Conf. Proc. **1134**, 22 (2009).

[15] D. J. Gross and A. Neveu, Phys. Rev. D **10**, 3235 (1974).

[16] C. L. Kane and E. J. Mele, Phys. Rev. Lett. **95**, 226801 (2005).

[17] A. J. Heeger, S. Kivelson, J. R. Schrieffer, and W. P. Su, Rev. Mod. Phys. **60**, 781 (1988).

[18] F. F. Assaad, Phys. Rev. B **71**, 075103 (2005).

[19] V. Ayyar and S. Chandrasekharan, arXiv:1410.6474.

[20] T. Yoshida, R. Peters, S. Fujimoto, and N. Kawakami, Phys. Rev. Lett. **112**, 196404 (2014).

[21] A. G. Abanov and P. B. Wiegmann, Nucl. Phys. B **570**, 685 (2000).

[22] H. Levine, S. B. Libby, and A. M. M. Pruisken, Phys. Rev. Lett. **51**, 1915 (1983).

[23] H. Levine, S. B. Libby, and A. M. M. Pruisken, Nucl. Phys. B **240**, 30 (1984); **240**, 49 (1984); **240**, 71 (1984).

[24] A. M. M. Pruisken, M. A. Baranov, and M. Voropaev, arXiv:cond-mat/0101003.

[25] C. Xu and A. W. W. Ludwig, Phys. Rev. Lett. **110**, 200405 (2013).

[26] Z. Bi, A. Rasmussen, and C. Xu, arXiv:1309.0515.

[27] Y. Ran, A. Vishwanath, and D.-H. Lee, Phys. Rev. Lett. **101**, 086801 (2008).

[28] X.-L. Qi and S.-C. Zhang, Phys. Rev. Lett. **101**, 086802 (2008).

[29] D. J. Thouless, M. Kohmoto, M. P. Nightingale, and M. den Nijs, Phys. Rev. Lett. **49**, 405 (1982).

[30] Q. Niu, D. J. Thouless, and Y. S. Wu, Phys. Rev. B **31**, 3372 (1985).

[31] K. Ishikawa and T. Matsuyama, Z. Phys. C **33**, 41 (1986).

[32] G. E. Volovik, *The Universe in a Helium Droplet* (Clarendon Press, Oxford, 2003).

[33] Z. Wang, X.-L. Qi, and S.-C. Zhang, Phys. Rev. Lett. **105**, 256803 (2010).

[34] Z. Wang, X.-L. Qi, and S.-C. Zhang, Phys. Rev. B **85**, 165126 (2012).

[35] Z. Wang and S.-C. Zhang, Phys. Rev. X **2**, 031008 (2012).

[36] Z. Wang and S.-C. Zhang, Phys. Rev. B **86**, 165116 (2012).

[37] Y.-Z. You, Z. Wang, J. Oon, and C. Xu, Phys. Rev. B **90**, 060502(R) (2014).

[38] F. Assaad and H. Evertz, *World-line and Determinantal Quantum Monte Carlo Methods for Spins, Phonons and Electrons*, Lecture Notes in Physics Vol. 739 (Springer, Berlin, 2008).

[39] M. Hohenadler, Z. Y. Meng, T. C. Lang, S. Wessel, A. Muramatsu, and F. F. Assaad, Phys. Rev. B **85**, 115132 (2012).

[40] Z. Y. Meng, T. C. Lang, S. Wessel, F. F. Assaad, and A. Muramatsu, Nature (London) **464**, 847 (2010).

[41] In the original Gross-Neveu model introduced in Ref. [15], ϕ_{ab} is always an identity matrix. Here we use a generalized definition of the Gross-Neveu model.

[42] Equation (3) has four flavors of complex fermions, which can be written as 8 flavors of Majorana fermion chains up to a basis transformation, i.e., 8 copies of Kitaev's 1d topological SC.